

# Phy-Diff: Physics-guided Hourglass Diffusion Model for Diffusion MRI Synthesis<sup>\*</sup>

Juanhua Zhang<sup>1</sup>, Ruodan Yan<sup>2</sup>, Alessandro Perelli<sup>1</sup>, Xi Chen<sup>3</sup>, and Chao Li<sup>1,2,4,5</sup>✉

<sup>1</sup> School of Science and Engineering, University of Dundee

<sup>2</sup> Department of Applied Mathematics and Theoretical Physics, University of Cambridge

<sup>3</sup> Department of Computer Science, University of Bath

<sup>4</sup> Department of Clinical Neurosciences, University of Cambridge

<sup>5</sup> School of Medicine, University of Dundee

c1647@cam.ac.uk

**Abstract.** Diffusion MRI (dMRI) is an important neuroimaging technique with high acquisition costs. Deep learning approaches have been used to enhance dMRI and predict diffusion biomarkers through under-sampled dMRI. To generate more comprehensive raw dMRI, generative adversarial network based methods are proposed to include b-values and b-vectors as conditions, but they are limited by unstable training and less desirable diversity. The emerging diffusion model (DM) promises to improve generative performance. However, it remains challenging to include essential information in conditioning DM for more relevant generation, i.e., the physical principles of dMRI and white matter tract structures. In this study, we propose a physics-guided diffusion model to generate high-quality dMRI. Our model introduces the physical principles of dMRI in the noise evolution in the diffusion process and introduce a query-based conditional mapping within the diffusion model. In addition, to enhance the anatomical fine details of the generation, we introduce the XTRACT atlas as prior of white matter tracts by adopting an adapter technique. Our experiment results show that our method outperforms other state-of-the-art methods and has the potential to advance dMRI enhancement.

**Keywords:** Diffusion MRI · Image synthesis · Hourglass diffusion model · Physics informed deep learning.

## 1 Introduction

Diffusion MRI (dMRI) is an essential neuroimaging modality due to its sensitivity in probing white matter fibers and characterizing neurological diseases [17]. However, acquiring high-quality dMRI for sufficient fidelity remains challenging due to expensive acquisition costs. For example, the neurite orientation dispersion and density imaging (NODDI) sequence requires 90 diffusion gradients, which is time-consuming and infeasible for patients with severe conditions

<sup>\*</sup> J. Zhang and R. Yan contribute equally in this work

[42]. There is an increasing need to develop effective algorithms for dMRI enhancement to reduce acquisition costs.

Deep learning has achieved encouraging performance in medical image synthesis and super-resolution. Based on conventional MRI, various frameworks have been proposed with success, supporting the feasibility of deep learning enhancing dMRI. Several studies have proposed frameworks to estimate dMRI parametric maps from undersampled high-resolution dMRI. For instance, a CNN-based model was proposed to use a few dMRI directions to generate diffusion kurtosis imaging (DKI) and NODDI maps [10]. Further, other methods were proposed based on Graph Transformer and atlas-aided U-Net to synthesize dMRI biomarkers [3,16]. However, these methods use sparsely sampled dMRI to generate specific parametric maps without leveraging b-values and b-vectors from raw dMRI for more comprehensive image generation. Therefore, these methods require re-training when applied to generating other parametric maps.

To mitigate this challenge, generative adversarial network (GAN) based frameworks are proposed using b-values and b-vectors as conditions, promising to generate comprehensive raw dMRI. The generated images were further used to calculate downstream parametric maps [31]. Despite the success, GAN-based architectures are often limited by their inability to balance fine details and visual quality [1], which could be suboptimal for clinical diagnosis. Further, GANs capture less diversity in large-volume generation [5], which cannot meet real-world clinical needs to address patient individuality. In addition, GANs often demonstrate unstable training, challenged by gradient vanishing and mode collapse [2].

As a type of likelihood-based model, diffusion models (DM) promise to achieve better generation performance while addressing the limitations of GANs [5]. Mounting research has shown that DMs are successful in generating high-quality, complex, and diverse images [12,27], with properties of fixed training targets and easy scalability [18]. Despite the advantages, there remains an unmet need to enhance dMRI effectively due to several challenges: 1) dMRI is distinct from conventional MRI in underlying physics principles. Therefore, generating dMRI may require additional physics-informed modeling beyond image geometry. However, typical DMs only add or remove random Gaussian noise in the diffusion process; 2) It remains a significant challenge for DMs to preserve the anatomical structures that are essential to the efficacy of dMRI in assessing tissue microstructure and characterising diseases. This is particularly important for the white matter tract regions that dMRI mainly reflects; 3) It is desirable to improve DMs for generating dMRI in a controllable manner with multiple conditions required, which is essential for restoring anatomical details in dMRI [5].

We propose a DM-based generative model tailored for dMRI, promoting image translation from the baseline images without gradient applied, i.e.,  $b_0$  images. Specifically, we introduce a physics-guided noise evolution and a query-based condition mapping. To better preserve the structural integrity of white matter tracts in the synthesized dMRI, we introduce local conditions of the XTRACT

atlas, with 42 anatomical tracts constructed from over 1,000 subjects [38]. Our main contributions include:

- We develop a physics-guided diffusion model to synthesize high-quality dMRI. As far as we know, this is the first attempt to generate raw dMRI using the conditional diffusion model.
- We propose a physics-guided noise evolution process in the forward diffusion to reflect the noise characteristics inherent in dMRI, which could improve on traditional DMs adding Gaussian noise.
- We design a query-based conditional mapping in the reverse diffusion process, incorporating q-space sampling to enable continuous diffusion gradient mapping, allowing for better directional dMRI synthesis at a given gradient.
- We introduce XTRACT atlas [38] as anatomical prior in conditioning DM for preserving the fine details of tract. Inspired by the T2I-Adapter [23], we improve the model adaptability for more controllable image generation while incorporating multiple conditions.

According to experimental results, our model achieves state-of-the-art performance and could serve as a promising tool for dMRI enhancement.

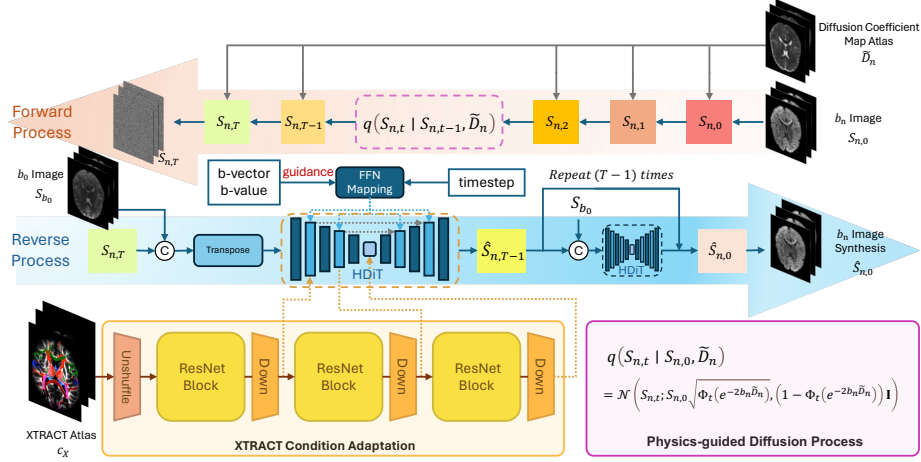


**Fig. 1. Model architecture.** The physics information ADC atlas  $\bar{D}_n$  interacts with the original image  $b_n$  during the forward process by the function  $q(S_{n,t} | S_{n,0}, \bar{D}_n)$ . After timesteps  $T$ , the image turns into the  $S_{n,T}$ . During the reverse process, HDiT predicts the added noise in each timestep in the pixel space, while using the b-vector, b-value as conditions via query-based conditional mapping. After training the noise prediction network, the XTRACT adapter is used to incorporate tractography structure  $c_x$ . By sampling from the learned pattern, the synthesized image  $\hat{S}_{n,0}$  is obtained.

## 2 Methodology

**Overview.** Fig.1 illustrates the model architecture. We propose a physics-guided diffusion process based on the framework of Denoising Diffusion Probabilistic Models (DDPM) [13], including a physics-guided noise evolution process and a query-based conditional mapping mechanism in the inference process. In the noise evolution process, Phy-Diff incorporates Apparent Diffusion Coefficient (ADC) map to learn the underlying noise representation in the synthesized dMRI data ( $b_n$ ) (detail in 2.1). During the reverse diffusion process, we employ a query-based conditional mapping technique that incorporate q-space sampling to guide the generation of  $b_n$  under the Hourglass Diffusion Transformer (HDiT) backbone, facilitating more precise directional dMRI synthesis (detail in 2.2). Furthermore, a XTRACT condition adaptation is designed to provide anatomical conditions guiding structural integrity of tracts in the synthesized dMRI (detail in 2.3).

### 2.1 Physics-guided Noise Evolution

The proposed physics-guided noise evolution process learn the underlying noise representation by leveraging an ADC atlas, where atlas referring to an average map. We first consider  $x_t$  as the  $t$ -th image representation, and the approximate posterior  $q(x_t | x_0)$ , representing the *diffusion process*, can be expressed as:

$$q(x_t | x_0) = \mathcal{N}(x_t; \sqrt{\bar{\alpha}_t}x_0, (1 - \bar{\alpha}_t)\mathbf{I}) \quad (1)$$

where,  $x_t$  is the noisy image at the timestep  $t$ ,  $x_0$  is the image that is expected to be generated, and  $\bar{\alpha}_t = \prod_{i=1}^t \alpha_i$ , and  $\alpha_i$  are hyper-parameters relevant to the variance. Thus,  $x_t$  can be computed by:

$$x_t = \sqrt{\bar{\alpha}_t}x_0 + \sqrt{1 - \bar{\alpha}_t}\epsilon, \quad \text{with } \epsilon \sim \mathcal{N}(0, \mathbf{I}) \quad (2)$$

where  $\epsilon$  represents the Gaussian noise schedule. By gradually increasing the proportion of noise and decreasing the proportion of content on the image, the final image will become completely noisy. The backbone network of DM gradually removes noise by predicting the noise changes at each timestep, ultimately restoring the original image.

However, the denoising mechanism of the standard DDPM may be more suitable for natural image generation, by multiplying the Gaussian noise with the uniform distributed variance, less considering specific structure of dMRI. To address this, we incorporate the diffusion physics inherent in dMRI into the process. Specifically, the diffusion physics information is integrated into the forward phase of DDPM:

$$S_n = S_0 e^{-b_n \mathcal{D}_n} + R(\mathcal{D}_n) \quad (3)$$

where  $\mathcal{D}_n$  represents diffusion coefficient,  $b_n$  is an arbitrary b-value, and  $S_n$  and  $S_0$  denote the signal intensities corresponding to the diffusion-weighted images

under b-values  $b_n$  and  $b_0$ , respectively. In order to approach the formula of DDPM as closely as possible, we developed a residual term  $R(\mathcal{D}_n)$  to effectively correct modeling errors caused by signal errors.

We then integrate this physical process (Eq. (3)) into the diffusion model architecture by assuming  $\tilde{\alpha}_t = \Phi_t(e^{-2b_n\mathcal{D}_n})$  and  $R(\mathcal{D}_n) = \sqrt{1 - \Phi_t(e^{-2b_n\mathcal{D}_n})}\epsilon$ , where  $\epsilon$  is the residual schedule. Specifically,  $\Phi_t(\cdot)$  refers to a transformation used to map the range of the function argument, making the diffusion process more stable. The goal is to solve for  $S_n$ . Therefore, we relax the restriction on  $\mathcal{D}_n$  and estimate that in the original equation as  $\tilde{\mathcal{D}}_n$  by introducing ADC atlas, which is expressed as:

$$\tilde{\mathcal{D}}_n = \sum_{i=1}^N \mathcal{D}_n^i = \frac{N \ln S_0 - \ln \prod_{i=1}^N S_n^i}{b_n} \quad (4)$$

where  $N$  denotes the number of all dMRI images  $\{S_n^0, S_n^1, \dots, S_n^N\}$  under the same b-value  $b_n$ , and  $S_0$  refers to the dMRI image under  $b = 0$ .

Consequently, our physics-guided noising mechanism is formulated as:

$$S_{n,t} = S_{n,0} \sqrt{\Phi_t(e^{-2b_n\tilde{\mathcal{D}}_n})} + \sqrt{1 - \Phi_t(e^{-2b_n\tilde{\mathcal{D}}_n})}\epsilon \quad (5)$$

The reverse process is also similar. Ultimately, the simplified form of the goal we need to optimize should be:

$$\mathcal{L}_{\text{simple}}(\theta) = \mathbb{E}_{\epsilon \sim \mathcal{N}(0,1)} \left[ \left\| \epsilon - D_\theta \left( S_{n,t}, t, \vec{b}_n, p_s, b_n \right) \right\|_2^2 \right] \quad (6)$$

where,  $t$  is the diffusion timestep. In addition, function  $D_\theta(\cdot)$  represents the backbone neural network model for noise prediction, and  $\vec{b}_n, p_s$  as well as  $b_n$  are the the b-vector, slice index and the b-value guidance, which will all be explained in detail in the following text.

## 2.2 Query-based Conditional Mapping

We introduce a query-based conditional mapping technique within the HDiT framework, to predict the noise at each timestep  $t$ . We employ the HDiT due to its efficiency in generating high-quality images in the pixel space because of the use of Neighborhood Attention (NA) [4].

The q-space condition is defined as the b-vector  $\vec{b}_n = (b_x, b_y, b_z)$  and its magnitude b-value  $|\vec{b}_n|$ , thus the q-space sampling, unlike integer scalar index categories, e.g., vector or slice position, requires tailored embedding to use as condition. Here, we develop a category embedding method for query-based conditional mapping, to further capture the directional information of the physics guidance  $\vec{D}_n$ . Since conventional positional embedding is only applicable to integer scalar index categories, b-vectors have to be normalized before mapping, overlooking the magnitude information specifying dMRI intensity. The proposed

embedding method clarify directional and magnitude categories based on real numbers. The real number embedding function  $\varepsilon_{real}(\cdot)$  can be briefly represented as:

$$\varepsilon_{real}(x) = f_{MLP} \left[ \frac{x}{|x|} \ln(|x| + 1) \right] \quad (7)$$

where  $f_{MLP}(\cdot)$  represents the multi-layer perceptron (MLP) function. This approach could benefit numerical stability.

Subsequently, guidance embeddings are integrated into the Transformer with  $N$  feed-forward network (FFN) blocks, using GEGLU [34]. The process includes enhancing the image with an MLP, three NA HDiT blocks for downsampling, a self-attention Transformer, and three more NA HDiT blocks for upsampling, all interacting with the guidances [4].

### 2.3 XTRACT Condition Adaptation

It is essential to preserve tract information for dMRI generation, thus we introduce the XTRACT, which includes 42 anatomically dissected tracts derived from over 1,000 human subjects. To better incorporate these tracts into DM conditioning, we employ a adapter technique inspired by [38], which could enhance the model adaptability for controllable image generation while incorporating multiple conditions.

Particularly, in order to fully adapt the XTRACT atlas to DM, it is necessary to exclude meaningless contents. We note that not all the image slices have tract on the XTRACT atlas. Therefore, we develop a module to enrich the empty positions. For those empty XTRACT, we combine  $S_{b_0}$  with the sum of the non-empty tracts, which can be simply expressed as:

$$c'_{X(i,j)} = \left( \sum_{k=1}^{42} c_{X(i,k)} + \xi \right) \cdot f_N(S_{b_0}) \quad (8)$$

where  $c_{X(i,j)}$  means the XTRACT condition in the  $i$ -th slice and the  $j$ -th tract,  $c'_{X(i,j)}$  is its replacement, and  $f_N$  represents the min-max normalization.

Subsequently, as illustrated in Fig. 1, we use a pixel unshuffle with a downsampling factor of 4 to downsample the input XTRACT atlas as conditions. Then, three classic ResNet blocks with each followed downsampling blocks are adopted. All features from each downsampling procedure are permuted to be consistent with each corresponding HDiT block for further addition.

## 3 Experiments and Results

### 3.1 Datasets and Preprocessing

We collected the dMRI data of 9 randomly selected subjects from Human Connectome Project (HCP) S1200 [6]. These subjects were divided into training, validation and testing sets at a ratio of 7:1:1. Each subjects contain images

**Table 1.** Performance on the HCP S1200 dataset. SSIM (%) and PSNR (dB) are listed in the test set. **Boldface** marks the top models. The b-values between arbitrary  $b_n$ ,  $b_n = 1000$ ,  $b_n = 2000$  and  $b_n = 3000$  as conditions are tested.

| Model                  | Arbitrary $b_n$   |                   | $b_n = 1000$      |                   | $b_n = 2000$      |                   | $b_n = 3000$      |                   |
|------------------------|-------------------|-------------------|-------------------|-------------------|-------------------|-------------------|-------------------|-------------------|
|                        | SSIM%             | PSNR              | SSIM%             | PSNR              | SSIM%             | PSNR              | SSIM%             | PSNR              |
| U-Net                  | 61.92±11.3        | 23.90±3.08        | 66.07±10.5        | 25.48±2.19        | 65.64±11.2        | 25.00±2.16        | 65.91±10.6        | <b>25.20±2.84</b> |
| U-Net++                | 61.89±9.34        | 23.21±2.83        | 65.74±10.8        | 25.20±2.43        | 66.31±10.3        | 24.49±2.19        | 65.18±12.3        | 24.21±3.03        |
| q-DL                   | 78.59±7.16        | 13.24±2.65        | 80.45±8.54        | 15.54±2.20        | 79.97±5.09        | 14.92±1.80        | 78.57±11.1        | 15.11±2.34        |
| q-DL 2D                | 63.41±21.25       | 21.93±3.38        | 67.88±18.6        | 25.41±2.85        | 70.63±16.66       | <b>25.52±2.94</b> | 66.10±21.7        | 24.78±2.70        |
| SMRI2DWI (CGAN)        | 32.12±8.89        | 20.71±3.15        | 33.32±7.48        | 24.53±2.38        | 34.66±6.10        | 24.02±2.56        | 34.67±7.80        | 24.06±2.78        |
| Latent Diffusion       | 70.69±8.66        | 21.31±2.11        | 69.96±9.08        | 21.00±1.47        | 68.69±7.59        | 20.89±1.51        | 69.26±8.50        | 21.31±1.66        |
| DDPM (HDiT)            | 81.92±5.41        | 22.70±2.26        | 86.78±3.94        | 25.72±1.95        | 82.71±4.92        | 23.36±2.02        | 81.19±6.51        | 22.26±3.01        |
| <b>Phy-Diff (Ours)</b> | <b>84.27±6.17</b> | <b>24.46±2.12</b> | <b>87.64±4.14</b> | <b>25.83±2.20</b> | <b>83.10±5.83</b> | 23.68±2.55        | <b>81.44±5.82</b> | 23.59±1.54        |

across b-value shells at 1000, 2000 and 3000  $s/mm^2$ , with each shell comprising 90 diffusion directions along with  $b_0$  images. Furthermore, 110 2D slices are extracted from each 3D images.

To ensure spatial consistency with XTRACT atlas, we first registered dMRI images to their corresponding T1-weighted images, followed by non-linearly transformed to the standard space by registering them to MNI-305 [7] using the Advanced Normalization Tools (ANTs). Additionally, we normalized all dMRI images, ADC atlas and XTRACT atlas, as well as b-vectors into the range of  $[-1, 1]$ , and padded all input images to ensure their resolution at  $256 \times 256$ .

### 3.2 Implementation Details

We implement the following hyperparameters: linear noise schedule; 1000 diffusion steps; noise variances at the range of  $\beta_1 = 10^{-4}$  and  $\beta_T = 0.02$ ; patch size of  $4 \times 4$ ; batch size of 32; AdamW optimizer with learning rate at  $5.0 \times 10^{-4}$ , weight decay at  $10^{-4}$ , betas at 0.9 and 0.95, eps at  $10^{-8}$ . The HDiT are implemented with three layers with dimensions of 128, 256, 512; 2 transformer blocks in each layer. The Adapter convolution channels are the same as HDiT dimensions, with the kernel size to 1. The model is trained in a NVIDIA A100-PCIE-40GB, and implemented through PyTorch.

### 3.3 Comparisons with SOTA and baselines

We compared our model with 5 state-of-the-art DWI synthesis approaches (Table 1): U-Net [33], U-Net++ [44], q-DL [10], q-DL (2D) [8], SMRI2DWI [31], LDM [32] and the original HDiT [4]. As conditioning is essential for our task, all models underwent slight modifications to incorporate basic conditioning, enabling them to utilize b-vectors and slice indices as conditions.

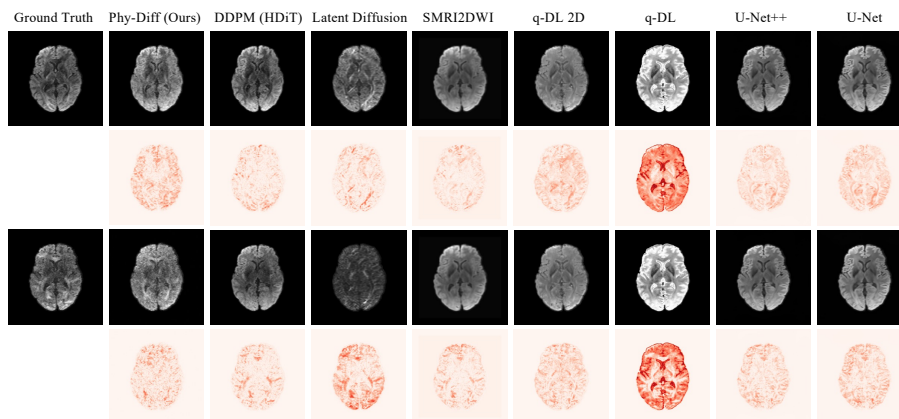
**Quantitative Results.** We generated dMRI based on any b-value and three different b-values, and the results showed that for any b-value, the performance of our Phy-Diff outperforms other models, with SSIM up to 52.15% and PSNR exceeding 11.22, which is the same to the situation when  $b_n = 1000$ ; In the cases

**Table 2.** Ablation studies on Arbitrary  $b_n$ . **Boldface** marks the top performance.

|                                     | SSIM%             | PSNR              |
|-------------------------------------|-------------------|-------------------|
| w/o Physics-guided noise evolution  | 84.24±5.86        | 24.12±2.53        |
| w/o XTRACT Adaptation               | 82.63±9.94        | 24.34±2.54        |
| w/o Query-based conditional mapping | 75.31±15.4        | 22.84±2.46        |
| <b>Phy-Diff (Ours)</b>              | <b>84.27±6.17</b> | <b>24.46±2.12</b> |

of  $b_n = 2000$  and  $b_n = 3000$ , SSIM can also surpass other models. However, PSNR is slightly inferior, which may be due to models with too low SSIM and too high PSNR excessively smoothing the image.

**Qualitative Results.** The first rows in Fig. 2 illustrate the synthesis results of arbitrary  $b_n$ , while the second row is the error map. From the generated images, Phy-Diff shows the most comparable results to ground truth, with minimal errors shown in the heat maps. Notably, Phy-Diff excels in reproducing white tracts, showcasing superior preservation of structural integrity.

**Fig. 2.** Examples of the generated dMRI. First row is the ground truth and synthesized image and second row is the error map.

### 3.4 Ablation Experiments

We evaluate the effectiveness of each component on the Phy-Diff by individually removing it. Our results (Table 2) show that each component contributes to the performance improvement, with query-based conditional mapping bringing a SSIM increase of 1.62dB and SSIM of 8.96%.



## 4 Conclusion

In this paper, we presents Phy-Diff, a DM-based dMRI generation model, with physics-guided noise evolution design, query-based category condition mapping, and XTRACT condition adapter. Our experiment demonstrates that Phy-Diff can achieve optimal performance under multiple b-values. Moreover, compared with other models, Phy-Diff demonstrates robust performance when accepting inputs with diverse b-vectors, b-values, and slices. Thus, Phy-Diff emerges as a powerful tool for dMRI generation, offering the potential to reduce acquisition time while maintaining high-quality results.

## References

1. Bau, D., Zhu, J.Y., Wulff, J., Peebles, W., Zhou, B., Strobelt, H., Torralba, A.: Seeing What a GAN Cannot Generate. In: 2019 IEEE/CVF International Conference on Computer Vision (ICCV). pp. 4501–4510 (Oct 2019). <https://doi.org/10.1109/ICCV.2019.00460>, <https://ieeexplore.ieee.org/document/9009809>, iSSN: 2380-7504
2. Berard, H., Gidel, G., Almahairi, A., Vincent, P., Lacoste-Julien, S.: A closer look at the optimization landscapes of generative adversarial networks. arXiv preprint arXiv:1906.04848 (2019)
3. Chen, G., Jiang, H., Liu, J., Ma, J., Cui, H., Xia, Y., Yap, P.T.: Hybrid Graph Transformer for Tissue Microstructure Estimation with Undersampled Diffusion MRI Data. In: Wang, L., Dou, Q., Fletcher, P.T., Speidel, S., Li, S. (eds.) Medical Image Computing and Computer Assisted Intervention – MICCAI 2022. pp. 113–122. Lecture Notes in Computer Science, Springer Nature Switzerland, Cham (2022). [https://doi.org/10.1007/978-3-031-16431-6\\_11](https://doi.org/10.1007/978-3-031-16431-6_11)
4. Crowson, K., Baumann, S.A., Birch, A., Abraham, T.M., Kaplan, D.Z., Shippole, E.: Scalable high-resolution pixel-space image synthesis with hourglass diffusion transformers (2024)
5. Dhariwal, P., Nichol, A.: Diffusion Models Beat GANs on Image Synthesis (Jun 2021). <https://doi.org/10.48550/arXiv.2105.05233>, <http://arxiv.org/abs/2105.05233>, arXiv:2105.05233 [cs, stat]
6. Essen, D.C.V., Smith, S.M., Barch, D.M., Behrens, T.E.J., Yacoub, E., Ugurbil, K.: The WU-Minn Human Connectome Project: An overview. *NeuroImage* **80**, 62–79 (2013). <https://doi.org/https://doi.org/10.1016/j.neuroimage.2013.05.041>, <https://www.sciencedirect.com/science/article/pii/S1053811913005351>
7. Fonov, V., Evans, A.C., Botteron, K., Almli, C.R., McKinstry, R.C., Collins, D.L.: Unbiased average age-appropriate atlases for pediatric studies. *NeuroImage* **54**(1), 313–327 (2011). <https://doi.org/https://doi.org/10.1016/j.neuroimage.2010.07.033>, <https://www.sciencedirect.com/science/article/pii/S1053811910010062>
8. Gibbons, E.K., Hodgson, K.K., Chaudhari, A.S., Richards, L.G., Majersik, J.J., Adluru, G., DiBella, E.V.: Simultaneous noddi and gfa parameter map generation from subsampled q-space imaging using deep learning. *Magnetic Resonance in Medicine* **81**(4), 2399–2411 (2019). <https://doi.org/https://doi.org/10.1002/mrm.27568>, <https://onlinelibrary.wiley.com/doi/abs/10.1002/mrm.27568>

9. Glasser, M.F., Sotiropoulos, S.N., Wilson, J.A., Coalson, T.S., Fischl, B., Andersson, J.L., Xu, J., Jbabdi, S., Webster, M., Polimeni, J.R., et al.: The minimal preprocessing pipelines for the human connectome project. *Neuroimage* **80**, 105–124 (2013)
10. Golkov, V., Dosovitskiy, A., Sperl, J.I., Menzel, M.I., Czisch, M., Sämann, P., Brox, T., Cremers, D.: q-Space Deep Learning: Twelve-Fold Shorter and Model-Free Diffusion MRI Scans. *IEEE Transactions on Medical Imaging* **35**(5), 1344–1351 (May 2016). <https://doi.org/10.1109/TMI.2016.2551324>, <https://ieeexplore.ieee.org/document/7448418>, conference Name: IEEE Transactions on Medical Imaging
11. Goodfellow, I.J., Pouget-Abadie, J., Mirza, M., Xu, B., Warde-Farley, D., Ozair, S., Courville, A., Bengio, Y.: Generative adversarial networks (2014)
12. Ho, J., Jain, A., Abbeel, P.: Denoising diffusion probabilistic models. arXiv:2006.11239 (2020)
13. Ho, J., Jain, A., Abbeel, P.: Denoising Diffusion Probabilistic Models. In: *Advances in Neural Information Processing Systems*. vol. 33, pp. 6840–6851. Curran Associates, Inc. (2020), <https://proceedings.neurips.cc/paper/2020/hash/4c5bcfec8584af0d967f1ab10179ca4b-Abstract.html>
14. Ho, J., Salimans, T.: Classifier-Free Diffusion Guidance (Jul 2022). <https://doi.org/10.48550/arXiv.2207.12598>, <http://arxiv.org/abs/2207.12598>, arXiv:2207.12598 [cs]
15. Jiang, L., Mao, Y., Wang, X., Chen, X., Li, C.: CoLa-Diff: Conditional Latent Diffusion Model for Multi-modal MRI Synthesis. In: Greenspan, H., Madabhushi, A., Mousavi, P., Salcudean, S., Duncan, J., Syeda-Mahmood, T., Taylor, R. (eds.) *Medical Image Computing and Computer Assisted Intervention – MICCAI 2023*. pp. 398–408. *Lecture Notes in Computer Science*, Springer Nature Switzerland, Cham (2023). [https://doi.org/10.1007/978-3-031-43999-5\\_38](https://doi.org/10.1007/978-3-031-43999-5_38)
16. Karimi, D., Gholipour, A.: Atlas-Powered Deep Learning (ADL) - Application to Diffusion Weighted MRI. In: Wang, L., Dou, Q., Fletcher, P.T., Speidel, S., Li, S. (eds.) *Medical Image Computing and Computer Assisted Intervention – MICCAI 2022*. pp. 123–132. *Lecture Notes in Computer Science*, Springer Nature Switzerland, Cham (2022). [https://doi.org/10.1007/978-3-031-16431-6\\_12](https://doi.org/10.1007/978-3-031-16431-6_12)
17. Le Bihan, D., Johansen-Berg, H.: Diffusion MRI at 25: Exploring brain tissue structure and function. *NeuroImage* **61**(2), 324–341 (Jun 2012). <https://doi.org/10.1016/j.neuroimage.2011.11.006>, <https://www.sciencedirect.com/science/article/pii/S1053811911012857>
18. Li, H., Yang, Y., Chang, M., Chen, S., Feng, H., Xu, Z., Li, Q., Chen, Y.: Srdiff: Single image super-resolution with diffusion probabilistic models. *Neurocomputing* **479**, 47–59 (2022)
19. Liu, P., Li, C., Schönlieb, C.B.: GANReDL: Medical Image Enhancement Using a Generative Adversarial Network with Real-Order Derivative Induced Loss Functions. In: Shen, D., Liu, T., Peters, T.M., Staib, L.H., Essert, C., Zhou, S., Yap, P.T., Khan, A. (eds.) *Medical Image Computing and Computer Assisted Intervention – MICCAI 2019*. pp. 110–117. *Lecture Notes in Computer Science*, Springer International Publishing, Cham (2019). [https://doi.org/10.1007/978-3-030-32248-9\\_13](https://doi.org/10.1007/978-3-030-32248-9_13)
20. Liu, X., Park, D.H., Azadi, S., Zhang, G., Chopikyan, A., Hu, Y., Shi, H., Rohrbach, A., Darrell, T.: More Control for Free! Image Synthesis with Semantic Diffusion Guidance (Dec 2022). <https://doi.org/10.48550/arXiv.2112.05744>, <http://arxiv.org/abs/2112.05744>, arXiv:2112.05744 [cs]

21. Mao, Y., Jiang, L., Chen, X., Li, C.: DisC-Diff: Disentangled Conditional Diffusion Model for Multi-contrast MRI Super-Resolution. In: Greenspan, H., Madabhushi, A., Mousavi, P., Salcudean, S., Duncan, J., Syeda-Mahmood, T., Taylor, R. (eds.) *Medical Image Computing and Computer Assisted Intervention – MICCAI 2023*. pp. 387–397. Lecture Notes in Computer Science, Springer Nature Switzerland, Cham (2023). [https://doi.org/10.1007/978-3-031-43999-5\\_37](https://doi.org/10.1007/978-3-031-43999-5_37)
22. Mirza, M., Osindero, S.: Conditional generative adversarial nets (2014)
23. Mou, C., Wang, X., Xie, L., Wu, Y., Zhang, J., Qi, Z., Shan, Y., Qie, X.: T2I-Adapter: Learning Adapters to Dig out More Controllable Ability for Text-to-Image Diffusion Models (Mar 2023). <https://doi.org/10.48550/arXiv.2302.08453>, <http://arxiv.org/abs/2302.08453>, arXiv:2302.08453 [cs]
24. Müller-Franzes, G., Niehues, J.M., Khader, F., Arasteh, S.T., Haarbuerger, C., Kuhl, C., Wang, T., Han, T., Nebelung, S., Kather, J.N., et al.: Diffusion probabilistic models beat gans on medical images. arXiv preprint arXiv:2212.07501 (2022)
25. Müller-Franzes, G., Niehues, J.M., Khader, F., Arasteh, S.T., Haarbuerger, C., Kuhl, C., Wang, T., Han, T., Nebelung, S., Kather, J.N., Truhn, D.: Diffusion Probabilistic Models beat GANs on Medical Images. *Scientific Reports* **13**(1), 12098 (Jul 2023). <https://doi.org/10.1038/s41598-023-39278-0>, <http://arxiv.org/abs/2212.07501>, arXiv:2212.07501 [cs, eess]
26. Nash, C., Menick, J., Dieleman, S., Battaglia, P.W.: Generating images with sparse representations. arXiv:2103.03841 (2021)
27. Nichol, A.Q., Dhariwal, P.: Improved denoising diffusion probabilistic models. In: *International Conference on Machine Learning*. pp. 8162–8171. PMLR (2021)
28. Nir, T.M., Jahanshad, N., Villalon-Reina, J.E., Toga, A.W., Jack, C.R., Weiner, M.W., Thompson, P.M., (ADNI, A.D.N.I., et al.: Effectiveness of regional dti measures in distinguishing alzheimer’s disease, mci, and normal aging. *NeuroImage: clinical* **3**, 180–195 (2013)
29. van den Oord, A., Vinyals, O., Kavukcuoglu, K.: Neural discrete representation learning. arXiv:1711.00937 (2017)
30. Razavi, A., van den Oord, A., Vinyals, O.: Generating diverse high-fidelity images with VQ-VAE-2. arXiv:1906.00446 (2019)
31. Ren, M., Kim, H., Dey, N., Gerig, G.: Q-space Conditioned Translation Networks for Directional Synthesis of Diffusion Weighted Images from Multi-modal Structural MRI. In: de Bruijne, M., Cattin, P.C., Cotin, S., Padoy, N., Speidel, S., Zheng, Y., Essert, C. (eds.) *Medical Image Computing and Computer Assisted Intervention – MICCAI 2021*. pp. 530–540. Lecture Notes in Computer Science, Springer International Publishing, Cham (2021). [https://doi.org/10.1007/978-3-030-87234-2\\_50](https://doi.org/10.1007/978-3-030-87234-2_50)
32. Rombach, R., Blattmann, A., Lorenz, D., Esser, P., Ommer, B.: High-Resolution Image Synthesis with Latent Diffusion Models. In: *2022 IEEE/CVF Conference on Computer Vision and Pattern Recognition (CVPR)*. pp. 10674–10685. IEEE, New Orleans, LA, USA (Jun 2022). <https://doi.org/10.1109/CVPR52688.2022.01042>, <https://ieeexplore.ieee.org/document/9878449/>
33. Ronneberger, O., Fischer, P., Brox, T.: U-net: Convolutional networks for biomedical image segmentation (2015)
34. Shazeer, N.: Glu variants improve transformer (2020)
35. Sohl-Dickstein, J., Weiss, E.A., Maheswaranathan, N., Ganguli, S.: Deep unsupervised learning using nonequilibrium thermodynamics. arXiv:1503.03585 (2015)
36. Song, Y., Ermon, S.: Generative modeling by estimating gradients of the data distribution. arXiv:arXiv:1907.05600 (2020)

37. Van Nguyen, H., Zhou, K., Vemulapalli, R.: Cross-Domain Synthesis of Medical Images Using Efficient Location-Sensitive Deep Network. In: Navab, N., Hornegger, J., Wells, W.M., Frangi, A. (eds.) *Medical Image Computing and Computer-Assisted Intervention – MICCAI 2015*. pp. 677–684. Lecture Notes in Computer Science, Springer International Publishing, Cham (2015). [https://doi.org/10.1007/978-3-319-24553-9\\_83](https://doi.org/10.1007/978-3-319-24553-9_83)
38. Warrington, S., Bryant, K.L., Khrapitchev, A.A., Sallet, J., Charquero-Ballester, M., Douaud, G., Jbabdi, S., Mars, R.B., Sotiropoulos, S.N.: XTRACT - Standardised protocols for automated tractography in the human and macaque brain. *NeuroImage* **217**, 116923 (Aug 2020). <https://doi.org/10.1016/j.neuroimage.2020.116923>, <https://www.sciencedirect.com/science/article/pii/S1053811920304092>
39. Yang, Q., Li, N., Zhao, Z., Fan, X., Chang, E.I.C., Xu, Y.: MRI Cross-Modality Image-to-Image Translation. *Scientific Reports* **10**(1), 3753 (Feb 2020). <https://doi.org/10.1038/s41598-020-60520-6>, <https://www.nature.com/articles/s41598-020-60520-6>, number: 1 Publisher: Nature Publishing Group
40. Yu, B., Wang, Y., Wang, L., Shen, D., Zhou, L.: Medical Image Synthesis via Deep Learning. In: Lee, G., Fujita, H. (eds.) *Deep Learning in Medical Image Analysis : Challenges and Applications*, pp. 23–44. *Advances in Experimental Medicine and Biology*, Springer International Publishing, Cham (2020). [https://doi.org/10.1007/978-3-030-33128-3\\_2](https://doi.org/10.1007/978-3-030-33128-3_2), [https://doi.org/10.1007/978-3-030-33128-3\\_2](https://doi.org/10.1007/978-3-030-33128-3_2)
41. Zeng, K., Zheng, H., Cai, C., Yang, Y., Zhang, K., Chen, Z.: Simultaneous single- and multi-contrast super-resolution for brain mri images based on a convolutional neural network. *Computers in Biology and Medicine* **99**, 133–141 (2018). <https://doi.org/https://doi.org/10.1016/j.combiomed.2018.06.010>, <https://www.sciencedirect.com/science/article/pii/S0010482518301586>
42. Zhang, H., Schneider, T., Wheeler-Kingshott, C.A., Alexander, D.C.: NODDI: Practical *in vivo* neurite orientation dispersion and density imaging of the human brain. *NeuroImage* **61**(4), 1000–1016 (Jul 2012). <https://doi.org/10.1016/j.neuroimage.2012.03.072>, <https://www.sciencedirect.com/science/article/pii/S1053811912003539>
43. Zhang, L., Rao, A., Agrawala, M.: Adding Conditional Control to Text-to-Image Diffusion Models. In: *2023 IEEE/CVF International Conference on Computer Vision (ICCV)*. pp. 3813–3824. IEEE, Paris, France (Oct 2023). <https://doi.org/10.1109/ICCV51070.2023.00355>, <https://ieeexplore.ieee.org/document/10377881/>
44. Zhou, Z., Siddiquee, M.M.R., Tajbakhsh, N., Liang, J.: Unet++: A nested u-net architecture for medical image segmentation (2018)